# Rational Design of Binary Alloys for Catalytic Growth of Graphene via Chemical Vapor Deposition

**Yanglizhi Li** [1,2,3,†], **Luzhao Sun** [1,2,3,†] , **Haiyang Liu** [1,3], **Yuechen Wang** [1,2,3] **and Zhongfan Liu** [1,3,*]

1   Center for Nanochemistry, Beijing Science and Engineering Center for Nanocarbons, Beijing National Laboratory for Molecular Sciences, College of Chemistry and Molecular Engineering, Peking University, Beijing 100871, China; liylz-cnc@pku.edu.cn (Y.L.); sunlz-cnc@pku.edu.cn (L.S.); liuhy-cnc@pku.edu.cn (H.L.); wangyc-cnc@pku.edu.cn (Y.W.)
2   Academy for Advanced Interdisciplinary Studies, Peking University, Beijing 100871, China
3   Beijing Graphene Institute, Beijing 100095, China
*   Correspondence: zfliu@pku.edu.cn; Tel.: +86-010-62757157
†   These authors contributed equally to this work.

check for updates

**Abstract:** Chemical vapor deposition is the most promising technique for the mass production of high-quality graphene, in which the metal substrate plays a crucial role in the catalytic decomposition of the carbon source, assisting the attachment of the active carbon species, and regulating the structure of the graphene film. Due to some drawbacks of single metal substrates, alloy substrates have gradually attracted attention owing to their complementarity in the catalytic growth of graphene. In this review, we focus on the rational design of binary alloys, such as Cu/Ni, Ni/Mo, and Cu/Si, to control the layer numbers and growth rate of graphene. By analyzing the elementary steps of graphene growth, general principles are summarized in terms of the catalytic activity, metal–carbon interactions, carbon solubility, and mutual miscibility. Several challenges in this field are also put forward to inspire the novel design of alloy catalysts and the synthesis of graphene films bearing desirable properties.

**Keywords:** alloy catalyst; chemical vapor deposition; graphene; fast growth; layer number control

## 1. Introduction

The rise of graphene [1,2] has aroused a new upsurge in exploring its intriguing physical and chemical properties on a two-dimensional scale [3–9], as well as its unique applications superior to those of bulk materials [10–13]. As an essential prerequisite for both fundamental research and practical utilization, the facile, cost-effective, and well-controlled preparation of graphene films with desired structures and properties has indubitably become the pursuit of academia. After more than a decade of research, chemical vapor deposition (CVD), and in particular CVD based on the use of metal catalysts, has stood out owing to its considerable advantages in the mass production of high-quality graphene films, thereby paving the way for its commercialization [14–16].

During the CVD growth of graphene films, the metal substrates, which catalyze the decomposition of the carbon sources into active carbon species and the subsequent assembly of these species into graphene, play vital roles in regulating the structure and properties of the resulting film. In general, single metal catalysts can be divided into two categories. The first is represented by a metal with a low carbon solubility, such as Cu, which features the self-limited model for growth of monolayer graphene but suffers from a relatively low catalytic activity [17]. The second category is represented by Ni, which has a high carbon solubility and catalytic activity, and the segregation of inhomogeneous

multilayer graphene is a common phenomenon [18]. With the rapid development of market demand and downstream applications, higher requirements have been put forward for the efficient preparation of graphene for specific demands. For instance, precise layer number control during the CVD process is of significant interest because the properties of graphene drastically change with the number of layers and their respective stacking orders. More specifically, the well-known tunable bandgap [19], the twisted-angle-dependent van Hove singularities [20,21], and unconventional superconductivity [22,23] only exist in bilayer graphene (BLG) with specific stacking structures. Moreover, the process of commercialization requires the rapid and low-temperature preparation of single-crystal graphene films [24,25]. In this regard, alloy metal substrates, such as Cu/Ni [26], Ni/Mo [27], Cu/Si [28], Pt/Si [29], Ni/Au [30], Ni/Ti [31], and Cu/Co [32], which combine the advantages of the different metal components, provide more significant benefits than single metal catalysts in terms of bridging the aforementioned gap. Therefore, the rational design of alloy catalysts is leading to a new trend in the controlled growth of high-quality graphene materials [33].

In this review, we briefly introduce the elementary steps of graphene growth on metal substrates to illustrate how the properties of the metal catalysts (i.e., the catalytic activity and carbon solubility, etc.,) can affect the growth behavior of graphene. Subsequently, with a preliminary impression of the design principles for metal substrates, recent advances in two important research topics, i.e., the layer number control and the fast growth of CVD-grown graphene, are summarized to detail the superiority of the alloy catalysts. Finally, the remaining synthetic challenges in graphene synthesis are put forward to inspire further in-depth research.

## 2. Elementary Steps for Graphene Growth on Metal Catalysts

Generally, a complete graphene preparation process includes the following steps: (1) pretreatment of the metal substrates (such as polishing and coating); (2) heating and annealing to enable grain coarsening, surface reconstruction, or/and complete alloying of the metal substrates; (3) graphene growth (at ~1000 °C in most cases); (4) cooling stages that are closely related to the segregation and wrinkling phenomenon of graphene. Specifically, several refined elementary steps exist during the graphene growth stage. For example, the carbon sources undergo a partial gas-phase reaction and mass transport in the chamber of the CVD system, followed by adsorption and stepwise decomposition into active carbon species on the surface of the metal catalyst [34]. Subsequently, two possible destinations are available for the carbon species depending on the carbon solubility and the metal–carbon interactions. One is on-surface migration, together with subsequent nucleation and edge-attachment to realize surface-mediated graphene growth, as is usually observed on metals with a low carbon solubility [17]. The second is dissolution into bulk metals with a high carbon solubility at high temperatures, and segregation to form graphene during the cooling stages due to the decreased carbon solubility [35] (Figure 1). Following the selection of an appropriate metal substrate, the growth mode is also assigned, leaving a limited growth window for regulating the structures of CVD-grown graphene. For instance, the self-limited growth mode of graphene on Cu renders it a promising substrate for the growth of single-layer graphene films. However, the low carbon solubility hinders the formation of large-area uniform bilayer or multilayer graphene, and the relatively weak catalytic activity [36] usually leads to a low growth rate.

Fortunately, owing to the mutual solubility of many transitional metals, alloy substrates, which possess the combined advantages of multiple metal components, provide significantly more possibilities for the controllable growth of graphene upon adjusting the composition and proportion of each metal element. This is manifested in, but not limited to, the following aspects: (1) the catalytic activity of the catalyst can be enhanced to increase the growth rate of graphene by alloying a certain proportion of the metal with a high catalytic activity into the original single metal matrix; (2) the carbon solubility can be tuned for the layer number control of graphene films by carefully designing the proportion of each metal component; (3) the metal–graphene interaction could be modified by varying

the surface state of the metals after alloying. Therefore, the selection of metal elements and their relative contents are crucial in the design of binary alloy catalysts.
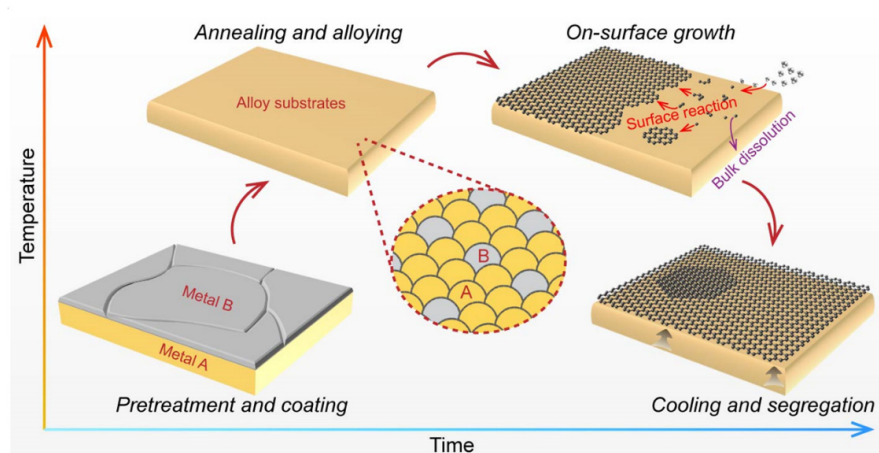


**Figure 1.** Process flow and elementary steps for graphene growth on metal substrates.

Generally speaking, there are two sources of the metals that make up alloy catalysts. One source includes the commonly used transition metals, including those with low carbon solubilities and/or weak metal–graphene interactions, such as Cu [17], Au [37], and Pt [38], in addition to those with high carbon solubilities and strong metal–graphene interactions, such as Ni [18] and Co [39], and those forming strong bonds with carbon, such as Ti [40,41] and Mo [42]. Another source is some nonmetallic elements that can form alloys with metals, such as Si. As mentioned above, the catalytic activity, carbon solubility, and interface interaction should be comprehensively considered to determine the elements present in an alloy (Figure 2). In addition, the miscibility of the elements is also an important prerequisite for the formation of alloys. Some physical properties of representative metals and Si crystals are listed in Table 1 for reference.
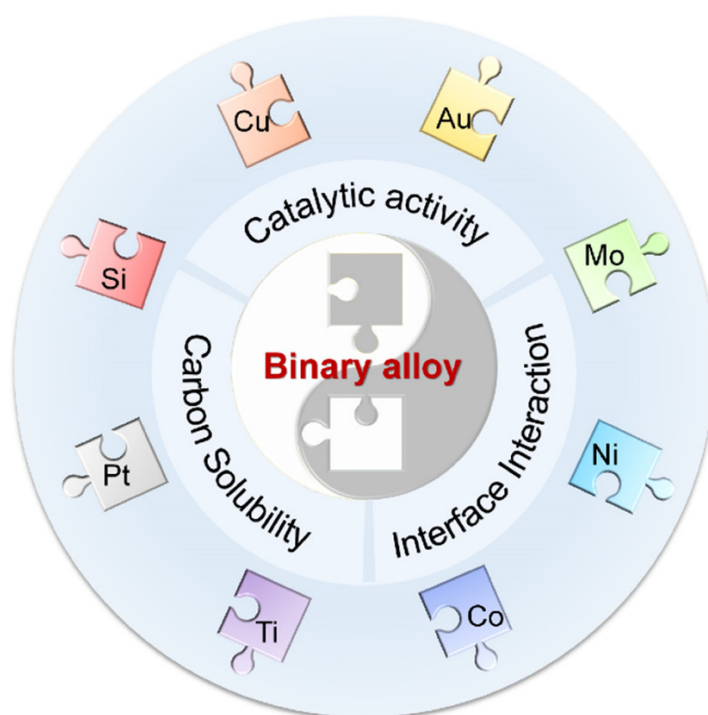


**Figure 2.** Rational design of binary alloy catalysts in terms of the catalytic activity, carbon solubility, and metal–graphene interactions.

**Table 1.** Summary of the physical properties of representative metals and Si crystals.

| Metal | Au | Co | Cu | Mo | Ni | Pt | Si | Ti |
|---|---|---|---|---|---|---|---|---|
| Carbon solubility (at.%, 1000 °C) [1] | 0.01 | 3.41 | 0.04 | 0.50 | 1.3 | 1.76 | - | 1.88 |
| Lattice constant (Å) [2] | 4.0786 | 3.5442 | 3.6150 | 3.1653 | 3.5238 | 3.9231 | 5.4305 | a = b = 2.953 c = 4.729 |
| Melting point (°C) [2] | 1064.18 | 1495 | 1084.62 | 2623 | 1455 | 1768.4 | 1414 | 1668 |
| Metal–graphene interaction [3] | $\pi$ = intact | - | $\pi$ = intact | - | $\pi$ = 2 eV | $\pi$ = intact | - | - |
| Electron configurations [4] | $5d^{10}6s^1$ | $3d^74s^2$ | $3d^{10}4s^1$ | $4d^55s^1$ | $3d^84s^2$ | $5d^96s^1$ | $3s^23p^2$ | $3d^24S^2$ |

[1] The carbon solubility values were obtained from Ref [43]. [2] The lattice constant and melting point values were obtained from Ref [44]. [3] The metal–graphene interactions were measured by the amount of downward shift of the $\pi$-band of graphene on the metal. "Intact" means a weak metal–graphene interaction (i.e., a linear dispersion at the Dirac point is still intact). These values were obtained from Ref [45]. [4] The catalytic activity is strongly influenced by the electron configuration. For instance, due to the absence of empty d orbitals, Cu has a low catalytic activity.

## 3. Layer Number Control of the Graphene Films

Monolayer graphene exhibits an ultrahigh carrier mobility, thermal conductivity, and mechanical strength; however, the lack of a band gap impedes its application in logic circuits [46]. One promising solution to open the band gap is the use of AB-stacked BLG, whose bandgap can be tuned using an external electric field [19]. In addition, exploration of the novel physical properties of twisted BLG is also in its initial stages [47,48]. Consequently, precise control of the layer number and stacking orders of CVD-grown graphene films is of great significance.

To control the layer number, one promising strategy is the use of the segregation technique proposed by Liu's group, where the as-formed graphene film originates from the carbon atoms dissolved in the bulk of the catalysts [35]. Therefore, binary alloys with adjustable carbon solubilities would be preferred, as in the case of the Cu/Ni alloy. More specifically, through the deposition of metal films (e.g., Ni and Cu) on $SiO_2$/Si substrates to form a sandwiched Cu/Ni/$SiO_2$/Si structure and subsequent high-temperature annealing, a Cu/Ni alloy can be formed, accompanied by the segregation of graphene films from the dissolved carbon atoms (Figure 3a). The plausible kinetic processes are summarized as follows. The dissolved carbon atoms undergo dynamic diffusion in the bulk, with some of them escaping onto the surface of the metal to initiate surface-mediated diffusion. Subsequently, the graphene domains nucleate at the defect or stepped sites of the catalysts and expand their size during the growth stage (Figure 3b). Indeed, this was the first time that the Cu/Ni alloy was used as the catalyst to prepare uniform graphene films (Figure 3c). The possibility of controlling the layer number of graphene films by the segregation technique was also explored, since this benefits from the fact that the atomic percentage of Ni can be precisely defined by controlling the thickness of the Ni films during the deposition process [26]. As shown in Figure 3d–k, a uniform monolayer graphene film with 95% coverage and BLG with 89% coverage were achieved by increasing the Ni content from 5.5 and 10.4%, respectively. A further increase in the Ni content gave rise to thicker graphene films. For the case of a low Ni content, the segregation behavior is approximately determined by Cu, where the weak metal–graphene interactions and low carbon solubility weaken the influence from the substrate, and result in the formation of single-layer graphene. The increase in the Ni content leads to the dissolution of a greater number of carbon atoms in the alloys to ultimately yield increased layer numbers of graphene.

Commercial polycrystalline Cu/Ni foils have also been employed to prepare graphene films with different layer distributions by regulating the growth temperature and cooling rate [49]. It was found that upon increasing the growth temperature from 930 to 1030 °C with a cooling rate of 100 °C/s, the layer numbers of graphene varied from the sub monolayer to 2–5 layers owing to the increased carbon solubility of the Cu/Ni substrates. Moreover, the cooling rate had a significant influence on determining the layer number of graphene. More specifically, lowering the cooling rate to 5 °C/s resulted in the formation of significantly thicker graphene films, which is in stark contrast with the case operating at a faster cooling rate. Furthermore, the growth mechanism of graphene grown on the Cu/Ni alloy was revealed by isotope labeling [50]. Through the sequential introduction of $^{12}CH_4$ and

$^{13}CH_4$ during the graphene growth process, BLG composed of the randomly mixed $^{12}C$ and $^{13}C$ was obtained on the surface of the $Cu_{90}Ni_{10}$ substrates, indicating that the surface precipitation mechanism dominated the Cu/Ni alloy. The influence of the nickel content and growth parameters on the number of graphene layers was investigated in detail at a later date [51–53].
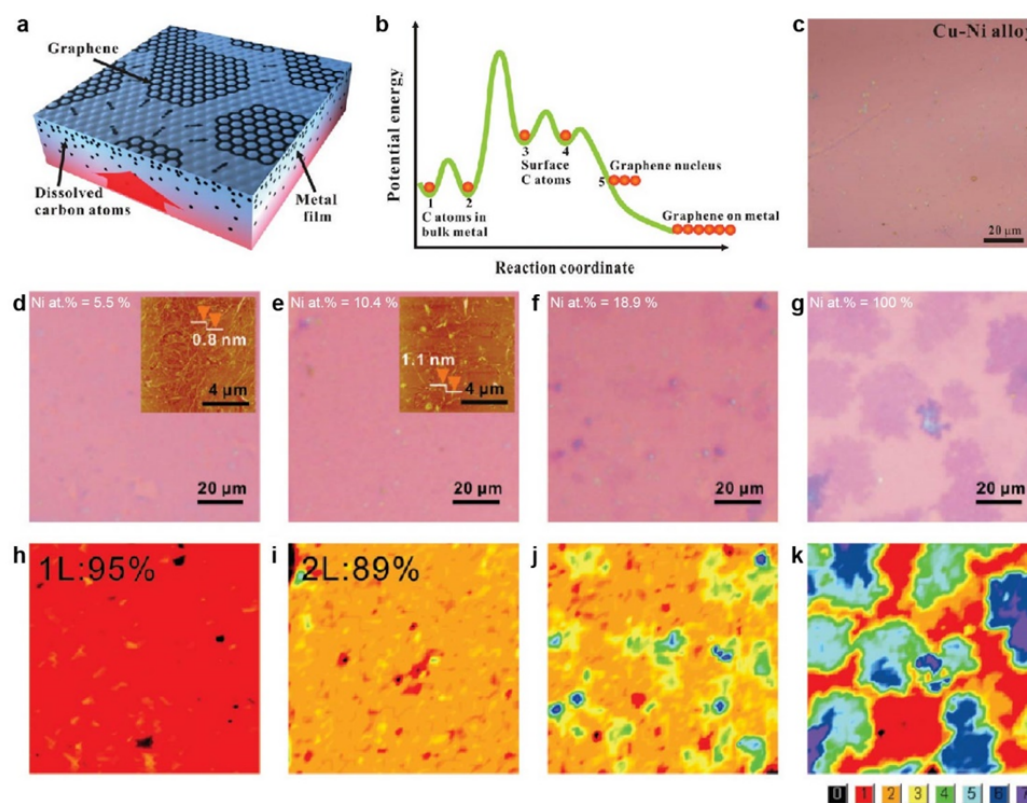


**Figure 3.** Segregation growth of graphene films on Cu/Ni alloy catalysts. (**a**) Schematic illustration of the segregation method to prepare the graphene films. (**b**) Energy profiles of the carbon atoms during the segregation process. (**c**) Optical image of the graphene film on $SiO_2$/Si grown using a Cu/Ni alloy catalyst. (**a**–**c**) Reprinted with permission from [35]. Copyright (2011), American Chemical Society. (**d**–**g**) Optical images of the graphene films grown from Cu/Ni alloy substrates with Ni atomic percentages of (**d**) 5.5%, (**e**) 10.4%, (**f**) 18.9%, and (**g**) 100%. The insets in (**d**,**e**) represent the corresponding atomic force microscopy images. (**h**–**k**) Layer number distributions obtained from the optical contrasts corresponding to (**d**–**g**), respectively. (**d**–**k**) Reprinted with permission from [26]. Copyright (2011), American Chemical Society.

In addition to the pursuit of the layer control, the preparation of BLG films with specific stacking sequences, such as AB-stacking BLG, has also attracted much attention. In 2014, Liu et al. achieved large uniform AB-stacking bilayer graphene (>98%) films on a $Cu_{75}Ni_{25}$ alloy through careful optimization of the surface carbon concentration [54]. The higher abundance of Cu on the surface compared to that in the bulk is considered to be a critical factor in decreasing the carbon diffusion in the bulk to enable the uniform growth of BLG. Later, in 2016, the Cu-vapor-assisted method was invented to reduce the effective content of Ni on the surface of the Cu/Ni alloy [55], thus further decreasing the on-surface growth rate of the first layer to enable more carbon diffusion into the catalyst. As a result, the second layer can segregate with a large coverage (>90%) to form AB-stacking BLG.

The crystal orientation of the Cu/Ni substrates was identified as another key factor in determining the stacking order of BLG by Ago's group [56]. In their work, a c-plane sapphire wafer was used as the epitaxial template for preparing $Cu_{80}/Ni_{20}(111)$ films. Subsequently, BLG films were formed in two consecutive processes: the first layer of graphene was formed in the high-temperature stage

following the surface growth mode, while the second layer segregated from the bulk during the cooling stage. Through careful characterization, four typical stacking configurations of the as-prepared BLG film with respect to the substrate were identified, namely aligned/aligned, 30°-rotated/aligned, 30°-rotated/30°-rotated, and aligned/30°-rotated configuration (Figure 4a), among which the proportion of the AB-stacking BLG accounted for 70–80%. According to density functional theory calculations, the graphene domains on the Cu/Ni(111) substrates possess a dominant orientation (0°) and a metastable orientation (30°), which explains the existence of the 30°-rotated configuration. Therefore, further exploration of the preparation of perfect AB-stacking BLG films is necessary. Recently, with the significant advances in the preparation of single-crystal Cu foils [57–59], single-crystal Cu/Ni(111) foils can be obtained by Ni plating on Cu foil and subsequent annealing [60] (Figure 4c,d). On the basis of the single-crystal catalysts that prevent non-uniform segregation at the grain boundary, uniform BLG films (>95% coverage and almost 100% AB-stacking configurations) and trilayer graphene (TLG) films (>60% coverage and almost 100% ABA-stacking configurations) were segregated from the Cu/Ni alloy, where the layer number control was found to depend strongly on the precise adjustment of the Ni content (Figure 4e–g).
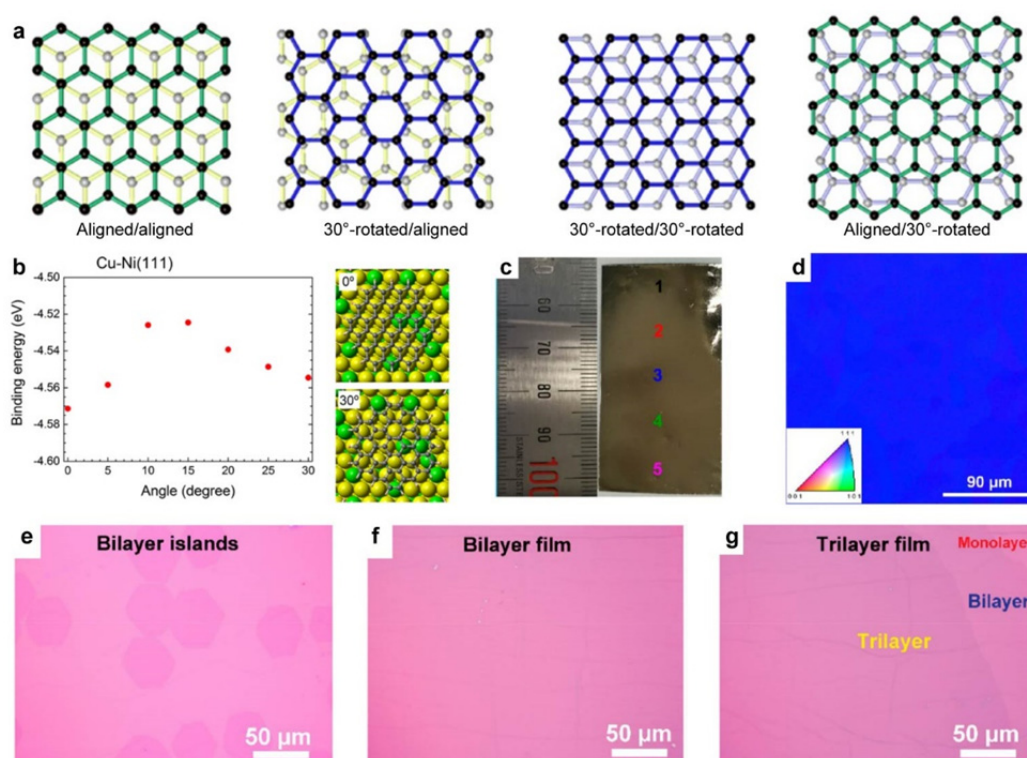


**Figure 4.** Growth of AB-stacking bilayer graphene (BLG) on Cu/Ni alloy catalysts. (**a**) Schematic illustration of the typical stacking orientations of BLG with respect to that of the substrate. (**b**) The binding energy of graphene on Cu/Ni(111) as a function of the relative orientation. (**a**,**b**) Reprinted with permission from [56]. Copyright (2016), American Chemical Society. (**c**) Photographic image of the Cu/Ni(111) foil. (**d**) EBSD IPF image of the Cu/Ni(111) foil. (**e**–**g**) Optical images of (**e**) the BLG islands, (**f**) a continuous BLG film, and (**g**) a TLG film. (**c**–**g**) Reprinted with permission from [60]. Copyright (2020), Springer Nature.

In addition to Cu/Ni substrates, some other alloy systems, such as Cu/Co, Pt/Si, and Cu/Si, are also strong candidates for controlling the layer number and/or stacking configurations of graphene. For instance, similar to Ni, Co has a moderate carbon solubility and partakes in strong interactions with graphene, and so can be integrated into the alloy catalyst. Lin et al. deposited Co films on the top of Cu foil to form the Co/Cu composite as the catalyst to control the layer number of the graphene film,

where the Co film served as the carbon capture layer while the inter-diffusion of Cu atoms into the Co layer regulated the carbon solubility of the Co layer [32].

Although extensive efforts have been made, several challenges still exist. For example, because the interlayer coupling between two layers of graphene is not sufficiently strong to prevent the influence of substrates with a non-uniform surface state, obtaining a continuous perfect AB-stacking BLG film remains a challenge. To address this issue, novel $Pt_3Si/Pt$ substrates were utilized as catalysts [61]. As shown in Figure 5a, a core–shell structure is clearly distinguished after the deposition of a Si film on polycrystalline Pt foils followed by high-temperature annealing. Given that the Pt core features a high melting point (1768.4 °C), while the $Pt_3Si$ shell melts at a relatively low temperature (830 °C), it tends to form a surface melting state, i.e., liquid $Pt_3Si$, at the growth temperature of graphene (1100–1025 °C), which is crucial for the interlayer epitaxial growth of uniform AB-stacking BLG. Following the on-surface growth of the first layer of graphene at 1100 °C (Figure 5b), the liquid $Pt_3Si$ provides a channel for carbon atoms precipitating from the Pt core to the surface. As a consequence, uniform BLG films were formed (Figure 5c). In addition, the smooth and uniform surface of the liquid $Pt_3Si$ renders the graphene domains easier to rotate on the liquid surface, allowing them to adopt the energy-favorable AB-stacking configuration (Figure 5d). These together contribute to the formation of a large AB-stacking BLG film. Very recently, significant progress has been made in synthesizing extremely uniform (100%) AB-stacking BLG and ABA-stacking TLG on a Cu/Si alloy [28]. Overall, four steps are involved in the preparation of graphene films: (1) The Cu/Si alloy is formed by annealing the Cu(111) film inside the quartz chamber at 900 °C, where the Si atoms come from the quartz tube; (2) the SiC layer is formed on the surface of the catalyst by introducing a carbon source ($CH_4$) into the chamber; (3) as the temperature increases to 1075 °C, graphene domains nucleate owing to the sublimation of Si atoms from the SiC layer; (4) the graphene domains expand with elongation of the annealing time, and finally merge into full graphene films (Figure 5e). Contrary to the segregation phenomenon on the Cu/Ni alloy, once the layer number of the initial graphene nuclei on the Cu/Si alloy is determined, each layer grows simultaneously at the same rate throughout the growth process, which is attributed to the diffusion-to-sublimation growth mode (Figure 5f). It was found that the layer numbers of graphene films can be precisely controlled by tuning the $CH_4$ concentrations during the process of SiC formation. Moreover, an optimal Si content (28.7%) exists in Cu/Si alloy catalysts to ensure the uniformity of the graphene layer, in which a small Si content will lead to a non-uniform thickness of the graphene films, while a larger Si content results in insufficient graphene growth due to the limited catalytic activity for decomposing the carbon source.

The aforementioned works focus on the controllable growth of bilayer or multilayer graphene with tunable carbon solubility on complementary alloy substrates. At the same time, the synthesis of absolute monolayer graphene within a wide growth window is also promising. Even on a Cu surface, strict monolayer graphene is not easy to acquire [62]. Given that the non-uniform multilayer graphene originates from non-equilibrium precipitation in metals with a high carbon solubility, such as Ni [63], the Mo component, which has a strong tendency to form molybdenum carbides (MoC) with carbon, was added into the Ni matrix to absorb the excess carbon dissolved in the bulk [27]. As shown in Figure 6a, the carbon atoms decomposed from the carbon source can either recombine into monolayer graphene on the Ni/Mo surface or diffuse into the bulk, where the latter route is not reversible because the carbon atoms are fixed in the bulk in the form of MoC. As a consequence, strict monolayer graphene films were realized as confirmed by transmission electron microscopy (TEM) and atomic force microscopy (AFM) characterizations (Figure 6b,c). The most fascinating advantage of growing monolayer graphene on a Ni/Mo alloy is its high tolerance to a wide range of growth parameters, including the growth time, C/H ratio in the carbon source, Ni/Mo ratio in the alloy, growth temperature, and cooling rate (Figure 6d). In addition to the Ni/Mo alloy, the Co/Mo alloy also shows similar properties.
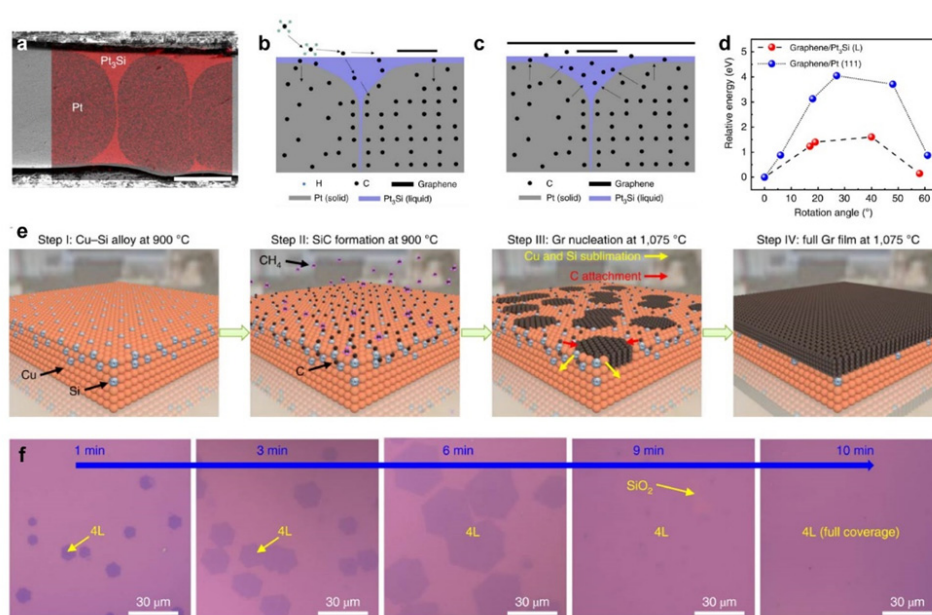
**Figure 5.** Growth of graphene films with well-controlled layer numbers on catalysts other than Cu/Ni. (**a**) Cross-section scanning electron microscopy (SEM) image and energy dispersive spectroscopy mapping of the $Pt_3Si/Pt$ foils. (**b**,**c**) Schematic illustration of uniform multilayer growth of (**b**) the first and (**c**) the second layer of graphene on a $Pt_3Si/Pt$ substrate. (**d**) The relative energies of graphene on Pt and $Pt_3Si$ as a function of the relative orientations. (**a**–**d**) Reprinted with permission from [61]. Copyright (2019), Springer Nature. (**e**) Schematic illustration of the uniform multilayer graphene films grown on the Cu/Si alloy catalyst. (**f**) Optical images of the time evolution of tetralayer graphene (Si/SiO$_2$ substrates) grown from the Cu/Si alloy. (**e**,**f**) Reprinted with permission from [28]. Copyright (2020), Springer Nature.
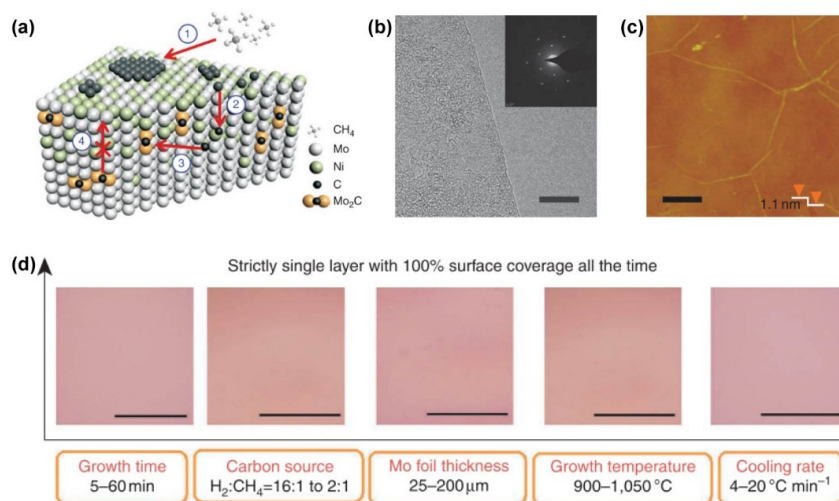


**Figure 6.** Growth of strict monolayer graphene on a Ni/Mo alloy. (**a**) Schematic illustration of the growth mechanism of graphene on a Ni/Mo alloy. (**b**) TEM and (**c**) AFM images of the monolayer graphene grown on a Ni/Mo alloy. Inset in (**b**) is the corresponding selected area electron diffraction pattern. (**d**) Optical images of the strict monolayer graphene synthesized using different growth parameters. Reprinted with permission from [27]. Copyright (2011), Springer Nature.

## 4. Low-Temperature and Fast Growth of Single-Crystal Graphene Films

As an important factors in the commercialization of graphene materials, reducing the time and energy consumption during the preparation process has attracted significant attention. Although Cu is the mainstream catalyst for the growth of monolayer graphene, its low catalytic activity limits the preparation efficiency. According to the elementary steps of the CVD growth described in the second section, two routes exist to compensate for the above deficiency: (1) optimization of the growth parameters, including the type [64] and supply process [65,66] of the carbon sources, gas flow [67], and trace auxiliary gas [68], etc.; (2) utilization of catalysts with higher catalytic activities and with the ability to maintain the monolayer of graphene. In this section, we focus on the latter route.

In general, the order of the catalytic activities of commonly used metal substrates is Ru~Rh~Ir > Co~Ni > Cu > Au~Ag [69]. The low catalytic activity of Cu can be attributed to the absence of unoccupied d orbitals, which play vital roles in forming metal–carbon bonds [14]. In 2015, Ding's group systematically investigated the binding energies, stabilities, and population of the hydrocarbon species ($CH_i$, i = 0, 1, 2, 3, 4) on different metal surfaces from a theoretical perspective [69]. It was found that binding of the $CH_i$ species with Ni, Ir, and Rh was stronger than that with Cu, indicating stronger metal–carbon interactions. Moreover, according to the population of the $CH_i$ species on different metal surfaces, the incomplete dehydrogenated CH species dominate the Cu surface at 800 and 1000 K (Figure 7b,c), and further elevation of the temperature facilitates the sufficient decomposition of the carbon source (Figure 7d,e). Meanwhile, the carbon monomers dominate the subsurface of Ni over the entire temperature range, and a large proportion of on-surface carbon monomers exist on the Ir and Rh substrates at high temperatures. These, together with the complete miscibility between Cu and Ni [70], reveal the feasibility of incorporating Ni atoms into the Cu matrix to enhance the catalytic activity.
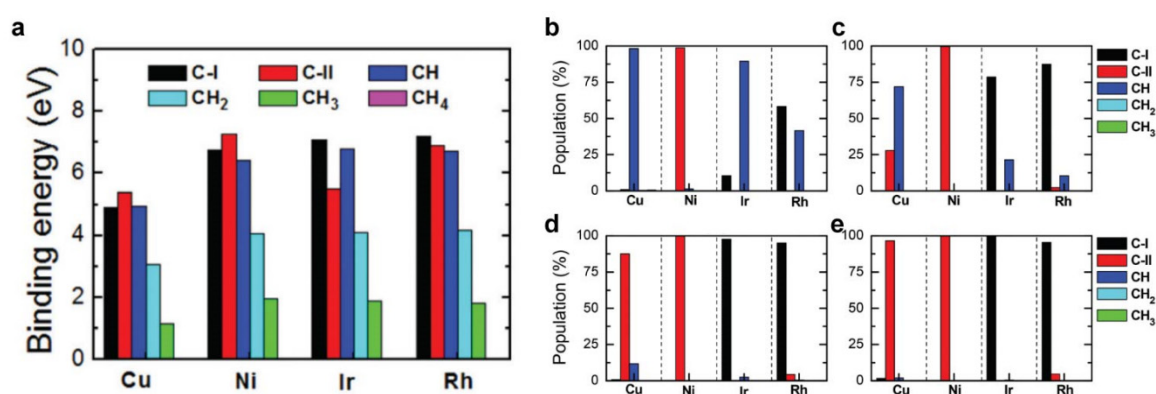


**Figure 7.** Theoretical calculation of the catalytic decomposition of $CH_4$ on typical metal substrates. (**a**) The binding energies of the various $CH_i$ (i = 0, 1, 2, 3, 4) species with Cu, Ni, Ir, and Rh. Note that when i = 0, the carbon specie can exist whether on metal surface (C-I) or subsurface (C-II). (**b–e**) Population of the various $CH_i$ species on the Cu(111), Ni(111), Ir(111), and Rh(111) surfaces at temperatures of (**b**) 800 K, (**c**) 1000 K, (**d**) 1200 K, and (**e**) 1400 K. Reprinted with permission from [69]. Copyright (2015), Royal Society of Chemistry.

As the commercial metal foils and films are almost polycrystalline in nature, the orientation distribution among different graphene domains on these substrates is wide, resulting in dense grain boundaries during the coalescence process [71,72]. To address this issue, one promising route is to reduce the nucleation density of graphene domains while accelerating the growth rate. In 2016, an isolated monolayer graphene with a large domain size (1.5-inch) was achieved in a short growth time (2.5 h) [73]. Such a low nucleation density is attributed to the following aspects: (1) A $Cu_{85}/Ni_{15}$ foil was adopted as the growth substrate instead of conventional Cu foil; (2) contrary to the common global carbon source feeding strategy (Figure 8a), local feeding of the carbon source was employed for nucleation control (Figure 8b). Moreover, the domain size of graphene increased linearly with time

on Cu/Ni, in contrast to that of saturation behavior on Cu (Figure 8c), owing to its higher catalytic activity for decomposition of carbon species (Figure 8d). Further in-depth exploration revealed that the nucleation density of graphene decreased with an increase in Ni content in the Cu/Ni alloy (Figure 8e), which is consistent with the decreased formation energy of adsorbed carbon atoms (Figure 8f) [74]. Note that a turnover of the formation energy from positive to negative appears at a Ni content of ~40%, which indicates that the carbon atoms prefer to remain independent and diffuse into the bulk rather than assembling into graphene on the surface at high Ni concentrations. Thus, there is a tradeoff between improving the catalytic activity and maintaining the on-surface growth of monolayer graphene.
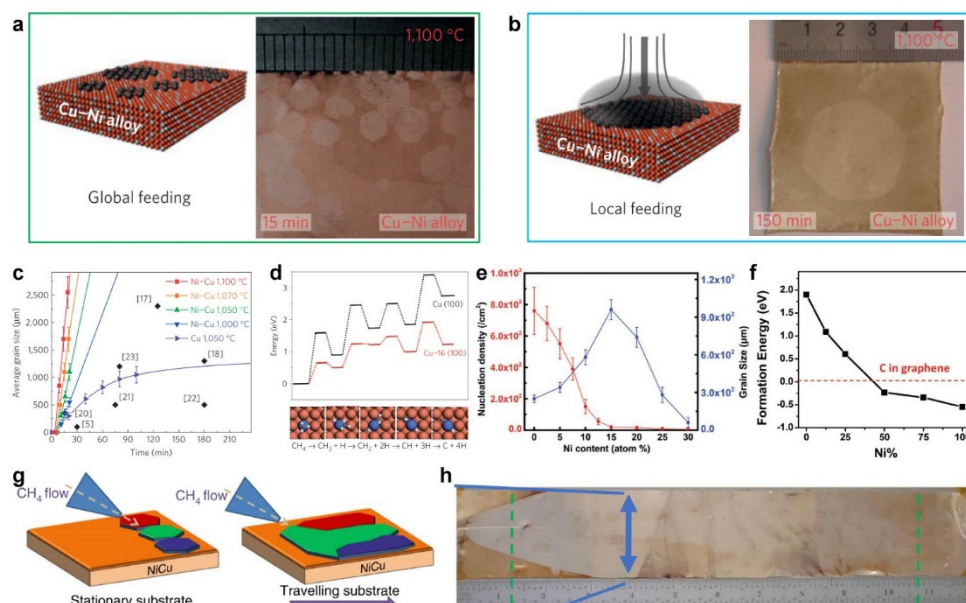


**Figure 8.** Fast growth of the single-crystal graphene films on a polycrystalline Cu/Ni alloy. (**a**,**b**) Schematic illustration (left panel) and corresponding photographic image (right panel) of the graphene grown on the Cu/Ni alloy with (**a**) global feeding and (**b**) local feeding of the carbon source. (**c**) Comparison of the growth rate of graphene on Cu and the Cu/Ni alloy at different temperatures. (**d**) Energy profiles of the decomposition of $CH_4$ on the Cu(100) and Cu/Ni(100) surfaces. (**a**–**d**) Reprinted with permission from [73]. Copyright (2016), Springer Nature. (**e**) The nucleation density and domain size of graphene, and (**f**) the calculated formation energy of the C atom as a function of the Ni content in the Cu/Ni alloy; (**e**,**f**) Reprinted with permission from [74]. Copyright (2018), Wiley-VCH. (**g**) Schematic illustration of the stationary growth (left) and evolutionary growth (right) of the graphene films. (**h**) Photographic image of the large single-crystal graphene films grown on polycrystalline Cu/Ni foils. (**g**,**h**) Reprinted with permission from [75]. Copyright (2018), Springer Nature.

On the basis of the local feeding strategy, an improvement named evolutionary selection growth was adopted to realize the continuous growth of single-crystal graphene films on polycrystalline Cu/Ni substrates [75]. In detail, a sharp carbon concentration gradient was created at the growth front by mixing the local carbon feeding ($CH_4$/Ar) and the high-velocity wind of the buffer gas ($H_2$/Ar) to avoid undesired graphene nucleation. This, together with the slow pulling of the Cu/Ni substrate, enabled the continuous attachment of the active carbon species onto the edge of the as-formed single-crystal graphene domains near the local feeding position (Figure 8g). As a consequence, a foot-long single-crystal graphene film was obtained (Figure 8h).

The availability of single-crystal Cu/Ni alloys further significantly promotes the preparation efficiency and the size of the single-crystal graphene films. Deng et al. successfully prepared 4-inch single-crystal $Cu_{90}Ni_{10}$(111) substrates via a two-step sputtering/annealing process [24]. Specifically, the Cu materials were initially sputtered onto the c-plane sapphire, and subsequently underwent

annealing to form a twin-free Cu(111) film. Then the second sputtering/annealing of the Ni film on Cu(111) led to the formation of a twin-free $Cu_{90}Ni_{10}$(111) alloy (Figure 9a,b), on which a 4-inch single-crystal graphene film can be obtained with a growth time of only 10 min. The significant improvement of the efficiency stems from two aspects: (1) owing to the matched symmetry and strong interactions between Cu/Ni(111) and graphene, the unidirectional growth of graphene domains and subsequent seamless stitching can be achieved with no need to control the nucleation density (Figure 9c); (2) the superior catalytic activity of the Cu/Ni alloy accelerates the growth rate of isolated graphene domains by 50 times compared to that of the Cu(111) (Figure 9d). The growth of graphene on $Cu_{90}/Ni_{10}$ alloy has been proved to be a surface-mediated process, as revealed by the isotope labeling technique (Figure 9e). Meanwhile, the 6-inch single-crystal Cu/Ni(111) wafers were also fabricated by a one-step sputtering/annealing method [25], where the polycrystalline Cu/Ni film was directly formed on c-plane sapphire from the Cu/Ni target at 200 °C, followed by annealing at 750 °C to eliminate the grain boundaries (Figure 9f). Owing to the excellent catalytic activity of the as-fabricated Cu/Ni(111), the single-crystal graphene films with undetectable defect-related band in Raman spectra can be obtained at only 750 °C (Figure 9g). In addition, the fast growth of aligned hexagonal graphene islands was also realized on single-crystal Cu/Ni(111) foils [76]. Very recently, the Cu/Ni(111) film has also been used as a catalytic substrate for the growth of wrinkle-free graphene film via a proton-assisted growth method [77].
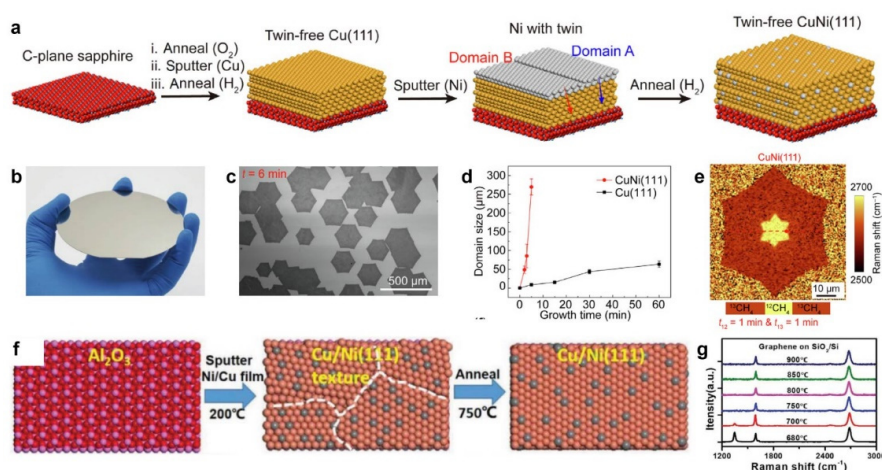


**Figure 9.** Low-temperature and fast growth of the single-crystal graphene films on single-crystal Cu/Ni(111) substrates. (**a**) Schematic illustration of fabrication of the single-crystal Cu/Ni(111) wafers via a two-step sputtering/annealing method. (**b**) Photographic image of the as-prepared single-crystal Cu/Ni(111) wafer. (**c**) SEM image of the epitaxial growth of the graphene domains on Cu/Ni(111). (**d**) Comparison of the domain size as a function of growth time on Cu/Ni(111) and Cu(111). (**e**) Raman 2D peak position mapping of a graphene domain on Cu/Ni(111). (**a**–**e**) Reprinted with permission from [24]. Copyright (2019), Elsevier. (**f**) Schematic illustration of fabrication of the single-crystal Cu/Ni(111) wafer via one-step sputtering. (**g**) Raman spectra of graphene films grown at different temperatures. (**f**,**g**) Reprinted with permission from [25]. Copyright (2019), Wiley-VCH.

In addition to the Cu/Ni alloy, it has been demonstrated that monolayer graphene can be produced on Ni/Au alloys at particularly low temperatures [30,78]. Moreover, the $Pt_3Si$/Pt composite also exhibits an excellent catalytic activity towards the fast growth (120 μm/min) of high-quality graphene film [29]. Nevertheless, the cost of using these noble metal-containing alloy catalysts should be considered in the batch production process. In terms of the practical applications, it is also worth trying to grow high-quality graphene on some specific functional alloys, such as biomedical alloy Ni/Ti [31]. The representative features of graphene grown on various alloy substrates are summarized in Table 2 for quick reference.

**Table 2.** Representative features of graphene grown on various alloy substrates.

| Purpose | Substrate | Key Parameters | Layer Number and Stacking Sequences | Domain Size | Growth Rate | Mobility ($cm^2 \cdot V^{-1} \cdot s^{-1}$) | Sheet Resistance ($\Omega$/sq) | Ref |
|---|---|---|---|---|---|---|---|---|
| Layer number control | Cu/Co foil | Controlling the Co content by varying the thickness of Co layer (80, 130, 205, 260, 400 nm, etc.) | 1–6 L | - | - | 926.6 (1 L), 836.4 (2 L), 804.5 (3 L), 664.2 (4 L), 428.3 (6 L) | 864 (1 L), 624 (2 L), 473 (3 L), 328 (4 L), 282 (6 L) | [32] |
| | Cu/Si film | Optimizing the Si content (28.7 at.%) and controlling the diluted $CH_4$ concentration (0.01%, 0.04%, 0.06%, 0.1%, etc.) | 1 L, 2 L (100% AB-Stacking), 3 L (100% ABA-Stacking), 4 L (ABCA and ABAB-stacking) | - | 10 min for full coverage | - | - | [28] |
| | Pt/Si foil | Optimizing the Si content and controlling a constant slow cooling rate | 2 L (AB-Stacking) | Millimeter size | 133 $\mu m \cdot min^{-1}$ | 2100 (at room temperature) | - | [61] |
| | Commercial $Cu_{70}/Ni_{30}$ foil | Controlling the growth temperature (975 °C, 1000 °C, 1030 °C) | 1 L, 2 L and few layers | - | - | - | 409 (1 L), 287 (2 L) | [49] |
| | Cu/Ni film | Controlling the Ni content (10%, 18%, 33%, 46%, 75% thickness ratio) | ~2 L, ~4 L, ~8 L, ~13, L~17 L, etc. | - | - | - | - | [53] |
| | Cu/Ni film | Controlling the Ni content (5.5 at.%, 10.4 at.%, 18.9 at.%, 100 at.%) | 1 L, 2 L, 2–4 L and few layers | - | - | - | - | [26] |
| | Cu/Ni film | Optimizing the Ni content (1200 nm Cu, 400 nm Ni) | 2L (98%AB-Stacking) | ~60 μm | - | 3450 (2 L), 1500 (3 L) | - | [54] |
| | Cu/Ni(111) foil | Controlling the Ni content (16.6 at.%, 20.3 at.%) and preparing the single-crystal Cu/Ni(111) foil | 2 L (95% AB-Stacking), 3 L (60% ABA-Stacking) | - | - | ~4000 (2 L, at room temperature) | - | [60] |
| | Cu/Ni foil | Placing a Cu foil above the Cu/Ni foil (Ni content 15 wt.%) | 2 L (90% AB-Stacking) | ~300 μm | 30 $\mu m \cdot min^{-1}$ (2 L) | - | - | [55] |
| | Cu/Ni(111) film | Preparing the single-crystal Cu/Ni(111) film and optimizing the Ni content (400 nm Cu, 100 nm Ni) | 2 L (90% AB-Stacking) | - | - | - | - | [56] |
| | Ni/Mo foil | Depositing Ni films (200 nm) on Mo foils (25 or 200 μm) | 1 L | - | - | 973 | - | [27] |
| Low temperature and fast growth | Cu/Ni foil | Optimizing the Ni content (15 wt%) and suitable growing temperature (1100 °C) and local precursor feeding | 1 L | 1.5 inch | 170 $\mu m \cdot min^{-1}$ (1100 °C) | 10,000–20,000 (at room temperature, h-BN substrate) | - | [73] |
| | Cu/Ni foil | Local carbon feeding and high-velocity wind of the buffer gas and pulling the substrates | 1 L | Decimeter size | 2.5 $cm \cdot h^{-1}$ | >10,000 | - | [75] |

**Table 2.** *Cont.*

| Purpose | Substrate | Key Parameters | Layer Number and Stacking Sequences | Domain Size | Growth Rate | Mobility ($cm^2 \cdot V^{-1} \cdot s^{-1}$) | Sheet Resistance ($\Omega$/sq) | Ref |
|---|---|---|---|---|---|---|---|---|
| | $Cu_{90}/Ni_{10}$(111) film | Optimizing the Ni content($Cu_{90}Ni_{10}$) and preparing single-crystal Cu/Ni(111)film | 1 L | 4 inch wafer | 50 $\mu m \cdot min^{-1}$, 10 min for full coverage | - | - | [24] |
| | $Cu_{85}/Ni_{15}$(111) film | Preparing the single-crystal Cu/Ni(111)film and optimizing the growth temperature (750 °C) | 1 L | 6 inch wafer | - | ~9700 (at 300K, h-BN substrate) | - | [25] |
| | Cu/Ni(111) foil | Preparing the single-crystal Cu/Ni(111) foil and optimizing the Ni content (<10 at.%) | 1 L | ~400 $\mu m$ (singe domain) | 70 $\mu m \cdot min^{-1}$, 5 min for full coverage | 5273 | 650 | [76] |
| | Ni/Au foil | Preparing Au-decorated Ni foil and growing graphene at ~600 °C | 1 L | ~20 $\mu m$ | - | 3000 | - | [78] |
| | Pt/Si foil | Forming silicated Pt to increase the on-surface dwell time of carbon atoms | 1 L | ~1.8 mm | 120 $\mu m \cdot min^{-1}$ | 5525 | - | [29] |

## 5. Conclusions and Outlook

In this review, we detailed the influence of metal substrates on the structures and properties of graphene films and summarized recent advances in the controllable growth of graphene films on binary alloy catalysts. More specifically, we note that the catalytic activity, carbon solubility, metal–graphene interaction, and mutual miscibility between metal components should be comprehensively considered for the rational design of binary alloy catalysts. In most cases, the binary alloy is composed of two metal components with complementary properties to avoid the shortcomings of the two elements. To control the layer number of graphene films, tuning the carbon solubility of the catalyst is the main concern, since the process of segregating carbon atoms from the bulk of the growth substrates is important for the formation of multilayer graphene. To meet the demand for the cost-effective preparation of single-crystal monolayer graphene, improving the catalytic activity and maintaining a low carbon solubility should simultaneously be taken into account.

Among the numerous binary alloy systems mentioned earlier, the Cu/Ni alloy appears to be the most promising catalyst for the mass production of high-quality graphene films owing to its low cost, easy availability, and complete mutual solubility between Cu and Ni, as well as its tunable carbon solubility and catalytic activity. Graphene films can grow on the Cu/Ni alloy either via the on-surface self-limited mode, the segregation mode, or the mix mode, depending on the Ni concentration. Other alloy systems, such as Ni/Mo, Cu/Si, and Pt/Si alloys, also show extraordinary advantages in controlling the number of layers of graphene.

However, despite substantial progress, several issues remain to be addressed. Preparing large-area uniform BLG or multilayer graphene with a specific twist angle remains a bottleneck. A further in-depth understanding of the metal–graphene interactions and exploration of the novel growth mechanism and alloy systems is therefore necessary for breaking the new ground on this issue. The superiority of single-crystal metal substrates over polycrystalline substrates has gradually become the consensus, and it would be expected that the following years may lead to new breakthroughs in the controllable growth of graphene and related two-dimensional materials based on single-crystal alloy substrates.

In addition, transferring graphene from metal substrate to a functional substrate is required for most of applications. In such process, chemical etching, electrochemical bubbling and direct mechanical delamination methods are usually employed to remove the growth substrates [79–82]. Therefore, the alloy substrates should be designed with the feature that can be easily etched or decoupled from the graphene films, which calls for more investigations in the future research.

## References

1.　Novoselov, K.S.; Geim, A.K.; Morozov, S.V.; Jiang, D.; Zhang, Y.; Dubonos, S.V.; Grigorieva, I.V.; Firsov, A.A. Electric field effect in atomically thin carbon films. *Science* **2004**, *306*, 666–669. [CrossRef]

2.　Geim, A.K.; Novoselov, K.S. The rise of graphene. *Nat. Mater.* **2007**, *6*, 183–191. [CrossRef]

3.　Nair, R.R.; Blake, P.; Grigorenko, A.N.; Novoselov, K.S.; Booth, T.J.; Stauber, T.; Peres, N.M.R.; Geim, A.K. Fine structure constant defines visual transparency of graphene. *Science* **2008**, *320*, 1308. [CrossRef] [PubMed]

4.  Novoselov, K.S.; Jiang, Z.; Zhang, Y.; Morozov, S.V.; Stormer, H.L.; Zeitler, U.; Maan, J.C.; Boebinger, G.S.; Kim, P.; Geim, A.K. Room-temperature quantum hall effect in graphene. *Science* **2007**, *315*, 1379. [CrossRef] [PubMed]

5.  Novoselov, K.S.; Geim, A.K.; Morozov, S.V.; Jiang, D.; Katsnelson, M.I.; Grigorieva, I.V.; Dubonos, S.V.; Firsov, A.A. Two-dimensional gas of massless Dirac fermions in graphene. *Nature* **2005**, *438*, 197–200. [CrossRef] [PubMed]

6.  Du, X.; Skachko, I.; Duerr, F.; Luican, A.; Andrei, E.Y. Fractional quantum Hall effect and insulating phase of Dirac electrons in graphene. *Nature* **2009**, *462*, 192–195. [CrossRef]

7.  Bolotin, K.I.; Ghahari, F.; Shulman, M.D.; Stormer, H.L.; Kim, P. Observation of the fractional quantum Hall effect in graphene. *Nature* **2009**, *462*, 196–199. [CrossRef]

8.  Lee, C.; Wei, X.; Kysar, J.W.; Hone, J. Measurement of the elastic properties and intrinsic strength of monolayer graphene. *Science* **2008**, *321*, 385–388. [CrossRef]

9.  Balandin, A.A.; Ghosh, S.; Bao, W.; Calizo, I.; Teweldebrhan, D.; Miao, F.; Lau, C.N. Superior thermal conductivity of single-layer graphene. *Nano Lett.* **2008**, *8*, 902–907. [CrossRef]

10. Bae, S.; Kim, H.; Lee, Y.; Xu, X.; Park, J.-S.; Zheng, Y.; Balakrishnan, J.; Lei, T.; Ri Kim, H.; Song, Y.I.; et al. Roll-to-roll production of 30-inch graphene films for transparent electrodes. *Nat. Nanotechnol.* **2010**, *5*, 574–578. [CrossRef]

11. Schwierz, F. Graphene transistors. *Nat. Nanotechnol.* **2010**, *5*, 487–496. [CrossRef] [PubMed]

12. Kim, K.; Choi, J.-Y.; Kim, T.; Cho, S.-H.; Chung, H.-J. A role for graphene in silicon-based semiconductor devices. *Nature* **2011**, *479*, 338–344. [CrossRef] [PubMed]

13. Koppens, F.H.L.; Mueller, T.; Avouris, P.; Ferrari, A.C.; Vitiello, M.S.; Polini, M. Photodetectors based on graphene, other two-dimensional materials and hybrid systems. *Nat. Nanotechnol.* **2014**, *9*, 780–793. [CrossRef]

14. Lin, L.; Deng, B.; Sun, J.; Peng, H.; Liu, Z. Bridging the gap between reality and ideal in chemical vapor deposition growth of graphene. *Chem. Rev.* **2018**, *118*, 9281–9343. [CrossRef]

15. Yang, J. Towards large-scale and high-quality graphene films. *Acta Phys. Chim. Sin.* **2019**, *35*, 1043–1044. [CrossRef]

16. Lin, L.; Peng, H.; Liu, Z. Synthesis challenges for graphene industry. *Nat. Mater.* **2019**, *18*, 520–524. [CrossRef] [PubMed]

17. Li, X.; Cai, W.; An, J.; Kim, S.; Nah, J.; Yang, D.; Piner, R.; Velamakanni, A.; Jung, I.; Tutuc, E.; et al. Large-area synthesis of high-quality and uniform graphene films on copper foils. *Science* **2009**, *324*, 1312–1314. [CrossRef]

18. Reina, A.; Jia, X.; Ho, J.; Nezich, D.; Son, H.; Bulovic, V.; Dresselhaus, M.S.; Kong, J. Large area, few-layer graphene films on arbitrary substrates by chemical vapor deposition. *Nano Lett.* **2009**, *9*, 30–35. [CrossRef]

19. Zhang, Y.; Tang, T.-T.; Girit, C.; Hao, Z.; Martin, M.C.; Zettl, A.; Crommie, M.F.; Shen, Y.R.; Wang, F. Direct observation of a widely tunable bandgap in bilayer graphene. *Nature* **2009**, *459*, 820–823. [CrossRef]

20. Li, G.; Luican, A.; Lopes Dos Santos, J.M.B.; Castro Neto, A.H.; Reina, A.; Kong, J.; Andrei, E.Y. Observation of Van Hove singularities in twisted graphene layers. *Nat. Phys.* **2010**, *6*, 109–113. [CrossRef]

21. Yin, J.; Wang, H.; Peng, H.; Tan, Z.; Liao, L.; Lin, L.; Sun, X.; Koh, A.L.; Chen, Y.; Peng, H.; et al. Selectively enhanced photocurrent generation in twisted bilayer graphene with van Hove singularity. *Nat. Commun.* **2016**, *7*, 10699. [CrossRef] [PubMed]

22. Cao, Y.; Fatemi, V.; Demir, A.; Fang, S.; Tomarken, S.L.; Luo, J.Y.; Sanchez-Yamagishi, J.D.; Watanabe, K.; Taniguchi, T.; Kaxiras, E.; et al. Correlated insulator behaviour at half-filling in magic-angle graphene superlattices. *Nature* **2018**, *556*, 80–84. [CrossRef]

23. Cao, Y.; Fatemi, V.; Fang, S.; Watanabe, K.; Taniguchi, T.; Kaxiras, E.; Jarillo-Herrero, P. Unconventional superconductivity in magic-angle graphene superlattices. *Nature* **2018**, *556*, 43–50. [CrossRef] [PubMed]

24. Deng, B.; Xin, Z.; Xue, R.; Zhang, S.; Xu, X.; Gao, J.; Tang, J.; Qi, Y.; Wang, Y.; Zhao, Y.; et al. Scalable and ultrafast epitaxial growth of single-crystal graphene wafers for electrically tunable liquid-crystal microlens arrays. *Sci. Bull.* **2019**, *64*, 659–668. [CrossRef]

25. Zhang, X.; Wu, T.; Jiang, Q.; Wang, H.; Zhu, H.; Chen, Z.; Jiang, R.; Niu, T.; Li, Z.; Zhang, Y.; et al. Epitaxial growth of 6 in. single-crystalline graphene on a Cu/Ni (111) Film at 750 °C via chemical vapor deposition. *Small* **2019**, *15*, 1805395. [CrossRef]

26. Liu, X.; Fu, L.; Liu, N.; Gao, T.; Zhang, Y.; Liao, L.; Liu, Z. Segregation growth of graphene on Cu-Ni alloy for precise layer control. *J. Phys. Chem. C* **2011**, *115*, 11976–11982. [CrossRef]

27. Dai, B.; Fu, L.; Zou, Z.; Wang, M.; Xu, H.; Wang, S.; Liu, Z. Rational design of a binary metal alloy for chemical vapour deposition growth of uniform single-layer graphene. *Nat. Commun.* **2011**, *2*, 522–526. [CrossRef] [PubMed]

28. Nguyen, V.L.; Duong, D.L.; Lee, S.H.; Avila, J.; Han, G.; Kim, Y.M.; Asensio, M.C.; Jeong, S.Y.; Lee, Y.H. Layer-controlled single-crystalline graphene film with stacking order via Cu–Si alloy formation. *Nat. Nanotechnol.* **2020**. [CrossRef]

29. Babenko, V.; Murdock, A.T.; Koós, A.A.; Britton, J.; Crossley, A.; Holdway, P.; Moffat, J.; Huang, J.; Alexander-Webber, J.A.; Nicholas, R.J.; et al. Rapid epitaxy-free graphene synthesis on silicidated polycrystalline platinum. *Nat. Commun.* **2015**, *6*, 7536. [CrossRef]

30. Weatherup, R.S.; Bayer, B.C.; Blume, R.; Ducati, C.; Baehtz, C.; Schlögl, R.; Hofmann, S. In situ characterization of alloy catalysts for Low-temperature graphene growth. *Nano Lett.* **2011**, *11*, 4154–4160. [CrossRef]

31. Li, J.; Wang, G.; Geng, H.; Zhu, H.; Zhang, M.; Di, Z.; Liu, X.; Chu, P.K.; Wang, X. CVD growth of graphene on NiTi alloy for enhanced biological activity. *ACS Appl. Mater. Interfaces* **2015**, *7*, 19876–19881. [CrossRef]

32. Lin, T.; Huang, F.; Wan, D.; Bi, H.; Xie, X.; Jiang, M. Self-regulating homogenous growth of high-quality graphene on Co-Cu composite substrate for layer control. *Nanoscale* **2013**, *5*, 5847–5853. [CrossRef] [PubMed]

33. Yan, K.; Fu, L.; Peng, H.; Liu, Z. Designed CVD growth of graphene via process engineering. *Acc. Chem. Res.* **2013**, *46*, 2263–2274. [CrossRef]

34. Zhang, X.; Li, H.; Ding, F. Self-Assembly of carbon atoms on transition metal surfaces-chemical vapor deposition growth mechanism of graphene. *Adv. Mater.* **2014**, *26*, 5488–5495. [CrossRef] [PubMed]

35. Liu, N.; Fu, L.; Dai, B.; Yan, K.; Liu, X.; Zhao, R.; Zhang, Y.; Liu, Z. Universal segregation growth approach to wafer-size graphene from non-noble metals. *Nano Lett.* **2011**, *11*, 297–303. [CrossRef] [PubMed]

36. Wang, X.; Yuan, Q.; Li, J.; Ding, F. The transition metal surface dependent methane decomposition in graphene chemical vapor deposition growth. *Nanoscale* **2017**, *9*, 11584–11589. [CrossRef]

37. Nie, S.; Bartelt, N.C.; Wofford, J.M.; Dubon, O.D.; McCarty, K.F.; Thürmer, K. Scanning tunneling microscopy study of graphene on Au(111): Growth mechanisms and substrate interactions. *Phys. Rev. B* **2012**, *85*, 205406. [CrossRef]

38. Sutter, P.; Sadowski, J.T.; Sutter, E. Graphene on Pt(111): Growth and substrate interaction. *Phys. Rev. B* **2009**, *80*, 1–10. [CrossRef]

39. Eom, D.; Prezzi, D.; Rim, K.T.; Zhou, H.; Lefenfeld, M.; Xiao, S.; Nuckolls, C.; Hybertsen, M.S.; Heinz, T.F.; Flynn, G.W. Structure and electronic properties of graphene nanoislands on $C_O(0001)$. *Nano Lett.* **2009**, *9*, 2844–2848. [CrossRef]

40. Aizawa, T.; Souda, R.; Otani, S.; Ishizawa, Y.; Oshima, C. Bond softening in monolayer graphite formed on transition-metal carbide surfaces. *Phys. Rev. B* **1990**, *42*, 11469–11478. [CrossRef]

41. Aizawa, T.; Souda, R.; Otani, S.; Ishizawa, Y.; Oshima, C. Anomalous bond of monolayer graphite on transition-metal carbide surfaces. *Phys. Rev. Lett.* **1990**, *64*, 768–771. [CrossRef] [PubMed]

42. Wu, Y.; Yu, G.; Wang, H.; Wang, B.; Chen, Z.; Zhang, Y.; Wang, B.; Shi, X.; Xie, X.; Jin, Z.; et al. Synthesis of large-area graphene on molybdenum foils by chemical vapor deposition. *Carbon* **2012**, *50*, 5226–5231. [CrossRef]

43. Sung, C.-M.; Tai, M.-F. Reactivities of transition metals with carbon: Implications to the mechanism of diamond synthesis under high pressure. *Int. J. Refract. Met. Hard Mater.* **1997**, *15*, 237–256. [CrossRef]

44. Lide, D.R. *CRC Handbook of Chemistry and Physics*; CRC Press: Boca Raton, FL, USA, 2004.

45. Batzill, M. The surface science of graphene: Metal interfaces, CVD synthesis, nanoribbons, chemical modifications, and defects. *Surf. Sci. Rep.* **2012**, *67*, 83–115. [CrossRef]

46. Castro Neto, A.H.; Guinea, F.; Peres, N.M.R.; Novoselov, K.S.; Geim, A.K. The electronic properties of graphene. *Rev. Mod. Phys.* **2009**, *81*, 109–162. [CrossRef]

47. Gibney, E. How 'magic angle' graphene is stirring up physics. *Nature* **2019**, *565*, 15–18. [CrossRef]

48. Ahn, S.J.; Moon, P.; Kim, T.-H.; Kim, H.-W.; Shin, H.-C.; Kim, E.H.; Cha, H.W.; Kahng, S.-J.; Kim, P.; Koshino, M.; et al. Dirac electrons in a dodecagonal graphene quasicrystal. *Science* **2018**, *361*, 782–786. [CrossRef]

49. Chen, S.; Cai, W.; Piner, R.D.; Suk, J.W.; Wu, Y.; Ren, Y.; Kang, J.; Ruoff, R.S. Synthesis and characterization of large-area graphene and graphite films on commercial Cu–Ni alloy foils. *Nano Lett.* **2011**, *11*, 3519–3525. [CrossRef]

50. Wu, Y.; Chou, H.; Ji, H.; Wu, Q.; Chen, S.; Jiang, W.; Hao, Y.; Kang, J.; Ren, Y.; Piner, R.D.; et al. Growth mechanism and controlled synthesis of AB-stacked bilayer graphene on Cu-Ni alloy foils. *ACS Nano* **2012**, *6*, 7731–7738. [CrossRef]

51. Wan, D.; Lin, T.; Bi, H.; Huang, F.; Xie, X.; Chen, I.W.; Jiang, M. Autonomously controlled homogenous growth of wafer-sized high-quality graphene via a smart Janus substrate. *Adv. Funct. Mater.* **2012**, *22*, 1033–1039. [CrossRef]

52. Wang, G.; Zhang, M.; Liu, S.; Xie, X.; Ding, G.; Wang, Y.; Chu, P.K.; Gao, H.; Ren, W.; Yuan, Q.; et al. Synthesis of layer-tunable graphene: A combined kinetic implantation and thermal ejection approach. *Adv. Funct. Mater.* **2015**, *25*, 3666–3675. [CrossRef]

53. Choi, H.; Lim, Y.; Park, M.; Lee, S.; Kang, Y.; Kim, M.S.; Kim, J.; Jeon, M. Precise control of chemical vapor deposition graphene layer thickness using Ni x Cu 1−x alloys. *J. Mater. Chem. C* **2015**, *3*, 1463–1467. [CrossRef]

54. Liu, W.; Kraemer, S.; Sarkar, D.; Li, H.; Ajayan, P.M.; Banerjee, K. Controllable and rapid synthesis of high-quality and large-area bernal stacked bilayer graphene using chemical vapor deposition. *Chem. Mater.* **2014**, *26*, 907–915. [CrossRef]

55. Yang, C.; Wu, T.; Wang, H.; Zhang, G.; Sun, J.; Lu, G.; Niu, T.; Li, A.; Xie, X.; Jiang, M. Copper-vapor-assisted rapid synthesis of large ab-stacked bilayer graphene domains on Cu-Ni alloy. *Small* **2016**, *12*, 2009–2013. [CrossRef] [PubMed]

56. Takesaki, Y.; Kawahara, K.; Hibino, H.; Okada, S.; Tsuji, M.; Ago, H. Highly uniform bilayer graphene on epitaxial Cu-Ni(111) alloy. *Chem. Mater.* **2016**, *28*, 4583–4592. [CrossRef]

57. Xu, X.; Zhang, Z.; Dong, J.; Yi, D.; Niu, J.; Wu, M.; Lin, L.; Yin, R.; Li, M.; Zhou, J.; et al. Ultrafast epitaxial growth of metre-sized single-crystal graphene on industrial Cu foil. *Sci. Bull.* **2017**, *62*, 1074–1080. [CrossRef]

58. Jin, S.; Huang, M.; Kwon, Y.; Zhang, L.; Li, B.-W.; Oh, S.; Dong, J.; Luo, D.; Biswal, M.; Cunning, B.V.; et al. Colossal grain growth yields single-crystal metal foils by contact-free annealing. *Science* **2018**, *362*, 1021–1025. [CrossRef]

59. Li, Y.; Sun, L.; Chang, Z.; Liu, H.; Wang, Y.; Liang, Y.; Chen, B.; Ding, Q.; Zhao, Z.; Wang, R.; et al. Large single-crystal cu foils with high-index facets by strain-engineered anomalous grain growth. *Adv. Mater.* **2020**, *32*, 2002034. [CrossRef]

60. Huang, M.; Bakharev, P.V.; Wang, Z.-J.; Biswal, M.; Yang, Z.; Jin, S.; Wang, B.; Park, H.J.; Li, Y.; Qu, D.; et al. Large-area single-crystal AB-bilayer and ABA-trilayer graphene grown on a Cu/Ni(111) foil. *Nat. Nanotechnol.* **2020**, *15*, 289–295. [CrossRef]

61. Ma, W.; Chen, M.-L.; Yin, L.; Liu, Z.; Li, H.; Xu, C.; Xin, X.; Sun, D.-M.; Cheng, H.-M.; Ren, W. Interlayer epitaxy of wafer-scale high-quality uniform AB-stacked bilayer graphene films on liquid Pt3Si/solid Pt. *Nat. Commun.* **2019**, *10*, 2809. [CrossRef]

62. Luo, D.; Wang, M.; Li, Y.; Kim, C.; Yu, K.M.; Kim, Y.; Han, H.; Biswal, M.; Huang, M.; Kwon, Y.; et al. Adlayer-free large-area single crystal graphene grown on a Cu(111) foil. *Adv. Mater.* **2019**, *31*, 1903615. [CrossRef] [PubMed]

63. Zhang, Y.; Gomez, L.; Ishikawa, F.N.; Madaria, A.; Ryu, K.; Wang, C.; Badmaev, A.; Zhou, C. Comparison of graphene growth on single-crystalline and polycrystalline Ni by chemical vapor deposition. *J. Phys. Chem. Lett.* **2010**, *1*, 3101–3107. [CrossRef]

64. Sun, X.; Lin, L.; Sun, L.; Zhang, J.; Rui, D.; Li, J.; Wang, M.; Tan, C.; Kang, N.; Wei, D.; et al. Low-temperature and rapid growth of large single-crystalline graphene with ethane. *Small* **2018**, *14*, 1702916. [CrossRef] [PubMed]

65. Lin, L.; Sun, L.; Zhang, J.; Sun, J.; Koh, A.L.; Peng, H.; Liu, Z. Rapid growth of large single-crystalline graphene via second passivation and multistage carbon supply. *Adv. Mater.* **2016**, *28*, 4671–4677. [CrossRef] [PubMed]

66. Sun, L.; Lin, L.; Zhang, J.; Wang, H.; Peng, H.; Liu, Z. Visualizing fast growth of large single-crystalline graphene by tunable isotopic carbon source. *Nano Res.* **2017**, *10*, 355–363. [CrossRef]

67. Wang, H.; Xu, X.; Li, J.; Lin, L.; Sun, L.; Sun, X.; Zhao, S.; Tan, C.; Chen, C.; Dang, W.; et al. Surface monocrystallization of copper foil for fast growth of large single-crystal graphene under free molecular flow. *Adv. Mater.* **2016**, *28*, 8968–8974. [CrossRef]

68. Xu, X.; Zhang, Z.; Qiu, L.; Zhuang, J.; Zhang, L.; Wang, H.; Liao, C.; Song, H.; Qiao, R.; Gao, P.; et al. Ultrafast growth of single-crystal graphene assisted by a continuous oxygen supply. *Nat. Nanotechnol.* **2016**, *11*, 930–935. [CrossRef]

69. Shu, H.; Tao, X.M.; Ding, F. What are the active carbon species during graphene chemical vapor deposition growth? *Nanoscale* **2015**, *7*, 1627–1634. [CrossRef]

70. Massalski, T.B.; Murray, J.L.; Bennet, L.H.; Baker, H. *Binary Alloy Phase Diagrams: Volume 1*; ASM International: Novelty, OH, USA, 1986.

71. Huang, P.Y.; Ruiz-Vargas, C.S.; Van Der Zande, A.M.; Whitney, W.S.; Levendorf, M.P.; Kevek, J.W.; Garg, S.; Alden, J.S.; Hustedt, C.J.; Zhu, Y.; et al. Grains and grain boundaries in single-layer graphene atomic patchwork quilts. *Nature* **2011**, *469*, 389–392. [CrossRef]

72. Yazyev, O.V.; Chen, Y.P. Polycrystalline graphene and other two-dimensional materials. *Nat. Nanotechnol.* **2014**, *9*, 755–767. [CrossRef]

73. Wu, T.; Zhang, X.; Yuan, Q.; Xue, J.; Lu, G.; Liu, Z.; Wang, H.; Wang, H.; Ding, F.; Yu, Q.; et al. Fast growth of inch-sized single-crystalline graphene from a controlled single nucleus on Cu–Ni alloys. *Nat. Mater.* **2016**, *15*, 43–47. [CrossRef] [PubMed]

74. Liu, Y.; Wu, T.; Yin, Y.; Zhang, X.; Yu, Q.; Searles, D.J.; Ding, F.; Yuan, Q.; Xie, X. How low nucleation density of graphene on CuNi alloy is achieved. *Adv. Sci.* **2018**, *5*, 1700961. [CrossRef]

75. Vlassiouk, I.V.; Stehle, Y.; Pudasaini, P.R.; Unocic, R.R.; Rack, P.D.; Baddorf, A.P.; Ivanov, I.N.; Lavrik, N.V.; List, F.; Gupta, N.; et al. Evolutionary selection growth of two-dimensional materials on polycrystalline substrates. *Nat. Mater.* **2018**, *17*, 318–322. [CrossRef] [PubMed]

76. Huang, M.; Biswal, M.; Park, H.J.; Jin, S.; Qu, D.; Hong, S.; Zhu, Z.; Qiu, L.; Luo, D.; Liu, X.; et al. Highly oriented monolayer graphene grown on a Cu/Ni(111) alloy foil. *ACS Nano* **2018**, *12*, 6117–6127. [CrossRef] [PubMed]

77. Yuan, G.; Lin, D.; Wang, Y.; Huang, X.; Chen, W.; Xie, X.; Zong, J.; Yuan, Q.Q.; Zheng, H.; Wang, D.; et al. Proton-assisted growth of ultra-flat graphene films. *Nature* **2020**, *577*, 204–208. [CrossRef] [PubMed]

78. Weatherup, R.S.; Dlubak, B.; Hofmann, S. Kinetic control of catalytic CVD for high-quality graphene at low temperatures. *ACS Nano* **2012**, *6*, 9996–10003. [CrossRef]

79. Ma, L.P.; Ren, W.; Cheng, H.M. Transfer methods of graphene from metal substrates: A review. *Small Methods* **2019**, *3*, 1900049. [CrossRef]

80. Sun, L.; Lin, L.; Wang, Z.; Rui, D.; Yu, Z.; Zhang, J.; Li, Y.; Liu, X.; Jia, K.; Wang, K.; et al. A force-engineered lint roller for superclean graphene. *Adv. Mater.* **2019**, *31*, 1902978. [CrossRef]

81. Gao, L.; Ren, W.; Xu, H.; Jin, L.; Wang, Z.; Ma, T.; Ma, L.-P.; Zhang, Z.; Fu, Q.; Peng, L.-M.; et al. Repeated growth and bubbling transfer of graphene with millimetre-size single-crystal grains using platinum. *Nat. Commun.* **2012**, *3*, 699. [CrossRef]

82. Wang, Y.; Zheng, Y.; Xu, X.; Dubuisson, E.; Bao, Q.; Lu, J.; Loh, K.P. Electrochemical delamination of CVD-grown graphene film: Toward the recyclable use of copper catalyst. *ACS Nano* **2011**, *5*, 9927–9933. [CrossRef]